Page Not Available

PREFACE

This is a severely abridged version of a Rand Research Memorandum (RM-2012) originally released in November 1957 in classified form to the U.S. Air Force under Project RAND (the forerunner to the present Project AIR FORCE). It is the product of a feasibility study undertaken in the spring of 1957 by several members of the Rand technical staff and led by Merton Davies and Amrom Katz.

The report is being released at the present time to make available--if even in partial form--some of the products of Rand's early research into the potentials of space flight. The authors are grateful to the reviewers in the Office of the Under Secretary of Defense for Policy, whose careful reading of the original made it possible to declassify and release extended portions of this seminal work.

CONTENTS

*The original Research Memorandum contained no Appendix I.

[Sections I through III (pp. 1-8) deleted]

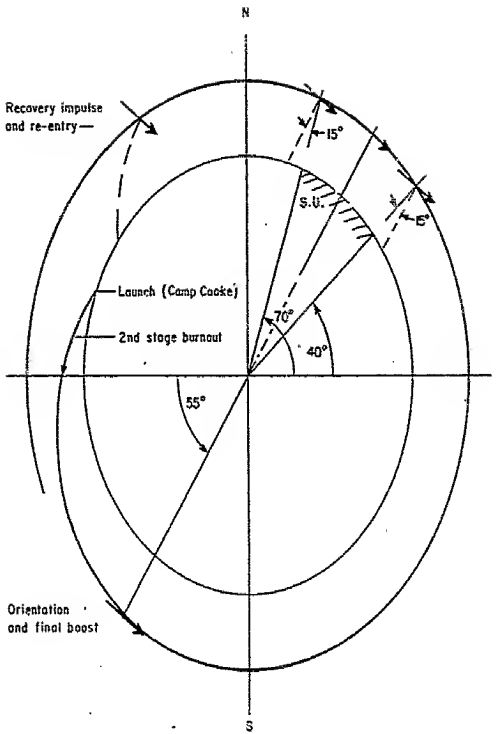

Fig. 3 — Schematic of trajectory and payload attitude

IV. THE ORBIT

ASCENT TRAJECTORY

The powered-ascent trajectory is effected by the combination of the Thor booster, with first-stage guidance preprogrammed for the autopilot, and the second-stage Vanguard using its autopilot in conjunction with components of the G.E. radio system.

During the period of coast to the design altitude of about 142 miles, the second stage, containing the spin-up and separation mechanism, orients and spins the third stage in preparation for the final velocity increment. A typical ascent trajectory is shown schematically in Fig. 3. The orientation, produced by the control jets (using residual helium) in the second stage, is to a pitch attitude such that the vehicle is parallel to the earth's surface at 55 degrees South (or North) latitude. After orientation, and before the third stage fires, the third stage and the payload are spun around their roll axis to the angular velocity required to stabilize the vehicle and provide the proper orientation of the payload.

The firing of the third stage separates it from the second stage and imparts the final velocity increment required to maintain a circular orbit. At third-stage burnout, a small separation device is fired, separating the payload and leaving it, properly oriented and spin-stabilized, in free space. (Appendix E)

V. THE VEHICLE

BOOSTER CONFIGURATION

The booster combination proposed for the early satellite is the Thor IRBM and the second stage of Vanguard, with a small solid rocket, similar in principle to the third stage of Vanguard, to provide a final orbital increment. The propulsion is thus provided by a liquid-liquid-solid combination. Table 2 is a summary of vehicle weights.

Table 2

Vehicle Weight Summary (lb)

Orbital payload	300
Third stage (solid)	350
Second stage (Vanguard 2nd)	4,730
Initial stage (Thor)	110,892

From a preliminary structural investigation it appears that the Thor airframe and its major components need not be modified for the satellite mission. The Thor autopilot and control system can be used for first-stage guidance, although there is some possibility that this system would

require some modification to offset the heavier load on the nose of the Thor and the increased loads during the ascent trajectory. For the satellite mission, the Thor inertial guidance system will not be required.

The basic airframe of the Vanguard second stage need not be modified for this application, with the exception of the aft interconnect structure, which will have to be designed to mate the 52-in. diameter Vanguard with the 84-in. diameter Thor nose cone. The guidance system of the second-stage Vanguard would be used in conjunction with G.E. (107A) components.

The size of the third stage has not been optimized. However, the Vanguard third stage is characteristic, in concept at least, of the type of solid propellant rocket that would be required for the present application. (Appendix F)

VI. TRACKING AND RECOVERY

Tracking will be required for essentially three reasons: to determine the orbit accurately enough for coordination of payload data; to trigger the braking rocket at the proper time for the descent; and to establish the descent path so that the impact point can be located.

The number of trackers required and the spacing between them is dictated partly by the guidance accuracy. To insure against guidance inaccuracies in launching, it is proposed that two or three trackers be used in an arrangement which places them generally with about a 200-mi separation on a line normal to the orbit.

A second factor that must be considered in determining the number and spacing of trackers is the deterioration of tracking accuracy at low angles above the horizon. It is highly important that the satellite pass close enough to at least one station so that sufficient tracking data can be obtained at angles of elevation greater than about 20 degrees. For a nominal satellite altitude of 142 mi, this requires that the satellite pass within roughly 5 degrees of the station, or within a ground range of about 350 mi. Again, two or three trackers at intervals of 200 mi normal to the orbit are dictated.

Because the satellite is to be placed on a polar orbit, these objectives can be met by a small number of trackers near one of the poles. It seems advisable to locate the tracking stations, say three of them, at a high northern latitude such as in Alaska or Canada. Spacing should be about 200 mi in longitude.

Tracking data would be in the form of two angles and a range to permit orbit prediction. The use of range information considerably relaxes

the requirement for angular accuracy. To obtain range, a transponder in the satellite is required. (Appendix G)

Descent from orbit is achieved by the command firing of a braking rocket in the satellite. Assume that the satellite is coming over the pole, that it is picked up by trackers in the north, and that an impact point in the Pacific is desired. The braking rocket is then fired forward and upward, imparting a downward and backward velocity impulse superimposed on the orbital velocity. The resulting velocity vector points downward, so that the vehicle is effectively in a ballistic trajectory comperable to the 'low-angle',i.e., lower-than-optimum, path of a long-range ballistic missile.

Tracking of the vehicle immediately after the beginning of descent establishes a predicted vacuum path. This, together with predicted atmospheric effects, makes it possible to predict the approximate impact area. The vehicle is protected against re-entry heating by a coating of suitable vaporizing material: 80 lb of fiberglass-reinforced plastic, such as is used on advanced designs of the ICBM nose cone and on the Jupiter nose cone, is suggested. Impact survival of the casing, payload, batteries, and beacon is made feasible by the proper selection and arrangement of structural components. Search aircraft are used to find and recover the payload. This means that the radio beacon must operate after water impact, and possibly that some type of dye marker should be released upon impact. (Appendix H)

[Sections VII and VIII, and Appendixes A and B (pp. 23-40), deleted]

Appendix C

ATTITUDE STABILIZATION

T. B. Garber

By spinning a vehicle about its longitudinal axis, the attitude of the body may be stabilized with respect to an inertial reference. It is of interest to examine the effect upon the angular motion of the body of external, applied torques. Such torques may arise from a number of sources: aerodynamic forces, the motion of components within the vehicle, or disturbances during propulsion. Figures 1 and 2 define some of the variables of interest.

In order to simplify the analysis, a circular orbit has been assumed. The rotational equations of motion of the vehicle, in body axes are:

$$\dot{\omega}_x + \frac{I_z - I_y}{I_x}\,\omega_y\,\omega_z = \frac{M_x}{I_x} \qquad \text{(a)}$$

$$\dot{\omega}_y + \frac{I_x - I_z}{I_y}\,\omega_x\,\omega_z = \frac{M_y}{I_y} \qquad \text{(b)} \qquad (1)$$

$$\dot{\omega}_z + \frac{I_y - I_x}{I_z}\,\omega_x\,\omega_y = \frac{M_z}{I_z} \qquad \text{(c)}$$

From Fig. 2 the relation between angular rates in body axes and the rate of change of the orientation angles may be deduced.

$$\dot{\theta} = \omega_y \cos\psi - \omega_z \sin\psi \qquad \text{(a)}$$

$$\dot{\gamma}\cos\theta = \omega_y \sin\psi + \omega_z \cos\psi \qquad \text{(b)} \qquad (2)$$

$$\dot{\psi} = \omega_x + \tan\theta\left[\omega_y \sin\psi + \omega_z \cos\psi\right] \qquad \text{(c)}$$

The first disturbances that will be considered are those due to residual control system errors. With a constant spin rate, ω_x, about the

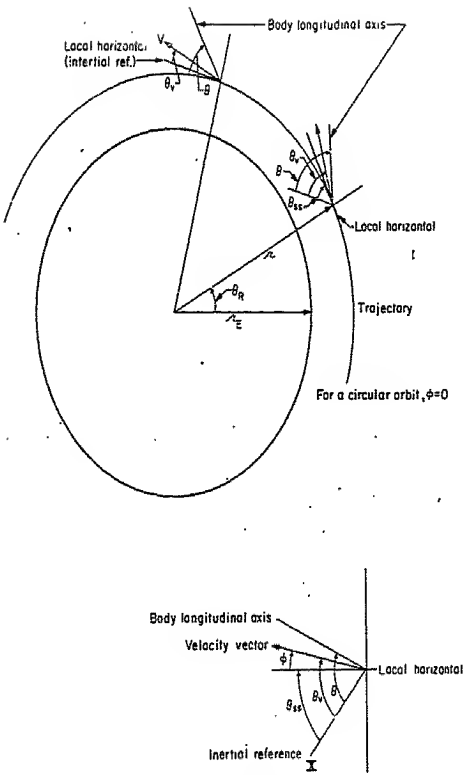

Fig. C-1 — Planar trajectory schematic

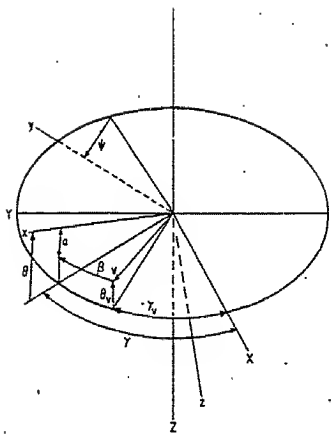

X, Y, Z, Inertial system

x Longitudinal axis of the vehicle

Fig. C-2—Orientation angles indicating angular positions of the velocity vector and longitudinal axes with respect to an inertial reference

longitudinal axis, and with no disturbing torques, Eq. (1, b and c) have the following solutions:

$$\omega_y = \omega_{y_0} \cos R_x \omega_x t + \omega_{z_0} \sin R_x \omega_x t \tag{3}$$

$$\omega_z = \omega_{z_0} \cos R_x \omega_x t - \omega_{y_0} \sin R_x \omega_x t \tag{4}$$

where $I = I_z = I_y$ and $R_x = \dfrac{I - I_x}{I}$

Introducing Eqs. (3) and (4) into Eq. (2) yields

$$\theta = \theta_0 + \epsilon_\theta - \frac{\epsilon_z}{R_x} + \frac{\epsilon_y}{R_x} \cos R_x t + \frac{\epsilon_\beta}{R_x} \sin R_x t \tag{5}$$

$$\gamma = \epsilon_\gamma + \frac{\epsilon_\beta}{R_x} - \frac{\epsilon_\theta}{R_x} \cos R_x t + \frac{\epsilon_z}{R_x} \sin R_x t \tag{6}$$

where $R_x = \dfrac{I_x \omega_x}{I}$, and the residual initial errors are denoted by ϵ with the appropriate subscript.

In obtaining Eqs. (5) and (6), it has been assumed that θ and γ are small angles, and that their product and the products of their time derivatives may be neglected. The validity of this assumption depends upon the magnitude of ω_x in Eq. (2,c) as compared to the remaining terms on the right hand side of the equation.

The angle of attack, α, is of interest since it indicates the departure of the longitudinal axis of the vehicle from the local horizontal. With the assumption that, over the range of θ_R of interest, γ and γ_v are small angles, the rigid body angular motion with respect to the velocity vector

in the absence of aerodynamic or other disturbing torques may be readily determined. (See Figs. 1 and 2.)

$$\alpha = +\dot{\theta}_{ss}t + \frac{\epsilon_{\dot{\beta}_0}}{R_x}\cos R_x t + \frac{\epsilon_{\dot{\alpha}}}{R_x}\sin R_x t + \left(\alpha_0 + \epsilon_\alpha - \frac{\epsilon_{\dot{\beta}}}{R_x}\right) \tag{7}$$

$$\beta = \frac{-\epsilon_{\dot{\alpha}}}{R_x}\cos R_x t + \frac{\epsilon_{\dot{\beta}}}{R_x}\sin R_x t + \epsilon_\beta + \frac{\epsilon_{\dot{\alpha}}}{R_x} \tag{8}$$

where α_0 is the desired attitude of the body at the initiation of the problem, and ϵ_α, ϵ_β, $\epsilon_{\dot{\alpha}}$, and $\epsilon_{\dot{\beta}}$ are the residual errors in α and β and the rates of change of those angles at the end of the orientation control period.

As would be expected, with all of the control errors equal to zero, the body longitudinal axis is stationary with respect to an inertial reference. However, an examination of the above equations indicates that with rate errors present, the usual precessional motion of a spinning body will occur.

Consider now the resultant error in θ and γ caused by this precession. For the error in $\dot{\theta}$, $\epsilon_{\dot{\theta}}$ values of 1°/sec to 3°/sec will be assumed. This performance is comparable to that obtained in the attitude control of current vehicles.* A similar value will be assumed for $\epsilon_{\dot{\gamma}}$. The angular position errors, ϵ_θ and ϵ_γ, might be as large as 2°. With θ and γ small angles, the vehicle orientation error due to residual rate errors is:

*Buchheim, R. W., 'Lunar Instrument Carrier--Attitude Stabilization,' RM-1730, June 4, 1956 (Unclassified).

$$\Delta A_{\theta,\gamma} = 1.41 \left\{ \left[\left(\frac{\epsilon_\theta}{R_x} \right)^2 + \left(\frac{\epsilon_\gamma}{R_x} \right)^2 \right] (1 - \cos R_x t) \right\}^{1/2} \qquad (9)$$

Figure 3 indicates the manner in which the envelope of $\Delta A_{\theta,\gamma}$ varies as a function of the parameter R_x.

At the end of the control and stabilization period the vehicle is boosted to orbital speed. With the thrust axis misaligned by a small angle, δ, a disturbing torque is applied to the craft.

$$M_y = T \cdot \ell_x \cdot \delta \qquad (10)$$

where T is the thrust, and ℓ_x is the moment arm.
With zero initial conditions, Eq. (1, b and c) now have the following solutions:

$$\omega_y = \frac{T \ell_x \delta}{R_z \omega_x I} \sin R_z \omega_x t \qquad (11)$$

$$\omega_z = \frac{T \ell_x \delta}{R_z \omega_x I} (\cos R_z \omega_x t - 1) \qquad (12)$$

where $0 \leq t \leq t_B$, and $R_z = \frac{I - I_x}{I}$.

It is assumed that the thrust is applied as a step function. Thus, Eqs. (11) and (12) are valid up to the end of the burning period, t_B. When $t > t_B$, ω_y and ω_z have the following form:

$$\omega_y = \frac{T \ell_x \delta}{I R_z \omega_x} \left[\sin R_z \omega_x t_B \cos R_z \omega_x t + (\cos R_z \omega_x t_B - 1) \sin R_z \omega_x t \right] \qquad (13)$$

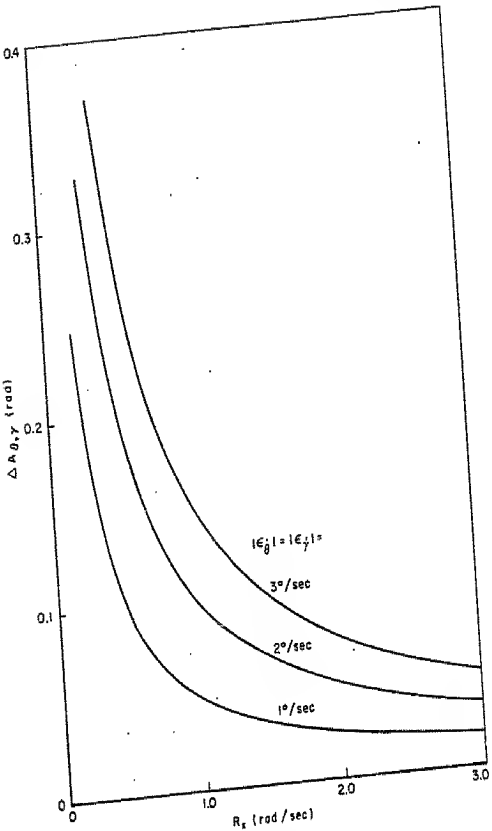

Fig. C-3—Total attitude error as a function of spin rate

$$\omega_z = \frac{T \ell_x \delta}{I R_z \omega_x} \left[(\cos R_z \omega_x t_B - 1) \cos R_z \omega_x t - \sin R_z \omega_x t_B \sin R_z \omega_x t \right] \quad (14)$$

where $t > 0$. (Zero time redefined at the end of burning.)

Introducing Eqs. (11) and (12) into Eq. (2, a,b and c) yields

$$\dot{\theta} = \frac{T \ell_x \delta}{I R_z \omega_x} P_1 \quad (a)$$

$$\dot{\gamma} \cos \theta = \frac{T \ell_x \delta}{I R_z \omega_x} P_2 \quad (b) \quad (15)$$

$$\dot{\psi} = \omega_z + \tan \theta \frac{T \ell_x \delta}{I R_z \omega_x} P_2 \quad (c)$$

where $0 \leq t \leq t_B$ and where

$$P_1 = \sin R_z \omega_x t \cos \psi + (1 - \cos R_z \omega_x t) \sin \psi$$

$$P_2 = \sin R_z \omega_x t \sin \psi - (1 - \cos R_z \omega_x t) \cos \psi$$

In the case of Eq. (15), the validity of a small angle solution depends upon the magnitude of $T \ell_x \delta / I R_z \omega_x$. It should be noted that this term may be reduced by reducing the thrust and increasing the burning time such that the total impulse remains constant.

A procedure that may be followed in obtaining solutions to Eq. (15, a, b and c) is to expand ψ in terms of a Taylor series in one of the parameters of $T \ell_x \delta / I R_z \omega_x$. Thus

$$\psi(t,\delta) = \psi_{\delta=0} + \left(\frac{\partial \psi}{\partial \delta}\right)_{\delta=0} \delta + \frac{1}{2} \left(\frac{\partial^2 \psi}{\partial \delta^2}\right)_{\delta=0} \delta^2 + \ldots \quad (16)$$

with a little manipulation, Φ may be eliminated from Eq. (15, b and c)

$$\ddot{\Psi} = \left(\frac{T\,\ell_x\,\delta}{I\,R_z\omega_x}\right)^2 P_1\,P_2 + (\dot{\Psi} - \omega_x)^2\,\frac{P_1}{P_2} + (\dot{\Psi} - \omega_x)\,\frac{\dot{P}_2}{P_2} \qquad (17)$$

From Eq. (17) the first three terms of the expansion of Eq. (16) may be determined. Thus:

$$\Psi_{\delta=0} = \omega_x t \qquad (a)$$

$$\left(\frac{\partial \Psi}{\partial \delta}\right)_{\delta=0} = 0 \qquad (b)$$

$$\left(\frac{\partial^2 \Psi}{\partial \delta^2}\right)_{\delta=0} = \left(\frac{T\,\ell_x}{I\,R_z\omega_x}\right)^2 \left\{ \frac{t\,(I + I_x)}{\omega_x I_x} + \frac{2}{\omega_x^2}\left[\frac{I\,(I_x - I)}{I_x^2} \sin R_x t \right.\right.$$

$$+ \left(\frac{I - I_x}{I_x}\right) \sin \omega_x t - \left(\frac{I\,(I_x + I)}{2\,I_x\,(I - I_x)}\right) \sin R_x \omega_x t \qquad (18)$$

$$- \frac{I}{2\,I_x} \sin (\omega_x + R_x)\,t + \frac{I^2}{4\,I_x^2} \sin 2\,R_x t \qquad (c)$$

$$\left.\left. + \frac{1}{4} \sin 2\,\omega_x t \right] \right\}$$

An examination of Eq. (18, a, b, and c) indicates that the first effect of the misalignment torque appears in the coefficient of δ^2, and consists of a term linear in time plus an oscillating component.

$$\psi \cong \left[\omega_x + \frac{1}{2} \left(\frac{T l_x \delta}{I R_z \omega_x} \right)^2 \frac{(I + I_x)}{\omega_x I_x} \right] t + \frac{1}{\omega_x^2} \left(\frac{T l_x \delta}{I R_z \omega_x} \right)^2 \psi_{osc.} \quad (19)$$

Introducing Eq. (19) into Eq. (15,a) and integrating yields

$$\theta = A_{R_x} \left\{ \cos \left[R_x + \mu \right] t - 1 \right\} + A_{\omega_x} \left\{ 1 - \cos \left[\omega_x + \mu \right] t \right\} + \frac{1}{2\omega_x^3} \left(\frac{T l_x \delta}{I R_z \omega_x} \right)^3 \ddot{z}_1(\psi_{osc.}) \quad (20)$$

where

$$A_{R_x} = \frac{\frac{T l_x \delta}{I R_z \omega_x}}{R_x + \frac{1}{2} \left(\frac{T l_x \delta}{I R_z \omega_x} \right)^2 \frac{(I + I_x)}{I_x \omega_x}}$$

$$A_{\omega_x} = \frac{\frac{T l_x \delta}{I R_z \omega_x}}{\omega_x + \frac{1}{2} \left(\frac{T l_x \delta}{I R_z \omega_x} \right)^2 \frac{(I + I_x)}{I_x \omega_x}}$$

$$\mu = \frac{1}{2} \left(\frac{T l_x \delta}{I R_z \omega_x} \right)^2 \frac{(I + I_x)}{I_x \omega_x}$$

From Eq. (20) it can be seen that the disturbing torque influences both the amplitude and the period of the pitch oscillation.

Combining Eq. (15,b and c) yields:

$$\dot{\gamma} = \pm \left\{ \left(\frac{T \ell_x \delta}{I R_x \omega_x} \right)^2 p_2^2 + (\dot{\psi} - \omega_x)^2 \right\}^{1/2} \tag{21}$$

Equation (21), upon consideration of Eq. (18) and Eq. (19), may be reduced to the following form:

$$\dot{\gamma} \cong \frac{T \ell_x \delta}{I R_x \omega_x} p_2 + \frac{1}{2\omega_x^2} \left(\frac{T \ell_x \delta}{I R_x \omega_x} \right)^3 \left[\frac{I}{I_x} (\cos R_x t - 1) + (1 - \cos \omega_x t) \right]^2 p_2 \tag{22}$$

Integrating Eq. (22) yields:

$$\gamma \cong A_{R_x} \sin \left[R_x + \mu \right] t \tag{23}$$

$$- A_{\omega_x} \sin \left[\omega_x + \mu \right] t + \frac{1}{2\omega_x^3} \left(\frac{T \ell_x \delta}{I R_x \omega_x} \right)^3 f_2 (\psi_{osc.})$$

If terms up to δ^2 are retained, then the pitch and yaw errors due to thrust misalignment at the end of the burning period are:

$$\Delta\theta_\delta = A_{R_x} \left[\cos (R_x + \mu) t_B - 1 \right] + A_{\omega_x} \left[1 - \cos (\omega_x + \mu) t_B \right] \tag{24}$$

and

$$\Delta\gamma_\delta = A_{R_x} \sin (R_x + \mu) t_B - A_{\omega_x} \sin (\omega_x + \mu) t_B \tag{25}$$

An examination of Eqs. (24) and (25) indicates that, for a known misalignment angle, $\Delta\theta_\delta$ and $\Delta\gamma_\delta$ may be constrained to be zero at t_B for any particular vehicle design, regardless of the value of A_{R_x} and A_{ω_x}. Thus,

$$R_x + \mu = \frac{n\pi}{t_B} \tag{26}$$

$$\omega_x + \mu = \frac{(n+2)\pi}{t_B} \tag{27}$$

where n is an even integer.

Introducing the expression for μ given with Eq. (20) into Eq. (27) yields:

$$\omega_x^4 - \frac{(n+2)\pi}{t_B}\omega_x^3 + \frac{1}{2}\left(\frac{T l_x \delta}{I R_x}\right)^2 \left(\frac{I + I_x}{I_x}\right) = 0 \tag{28}$$

The ratio, $\frac{I_x}{I}$ may be found in terms of ω_x and t_B by subtracting Eq. (26) from Eq. (27). Thus,

$$\omega_x^2 - \frac{(n+2)\pi}{t_B}\omega_x + \left(\frac{T l_x \delta t_B}{2\pi I}\right)^2 \left[\frac{\omega_x t_B - \pi}{\omega_x t_B - 2\pi}\right] = 0 \tag{29}$$

An approximate solution of Eq. (29) may be found by expanding ω_x in a Taylor series in δ.

$$\omega_x = \frac{(2+n)\pi}{t_B} - \frac{t_B}{(n+2)\pi}\left(\frac{n+1}{n}\right)\left(\frac{\nu l_x \delta}{2\pi I}\right)^2 \tag{30}$$

where ν is the total impulse.

The ratio $\frac{I_x}{I}$ is

$$\frac{I_x}{I} = 1 - \frac{2\pi}{\omega_x t_B} = \frac{n\pi - \frac{t_B^2}{(n+2)\pi}\left(\frac{\nu l_x \delta}{2\pi I}\right)^2\left(\frac{n+1}{n}\right)}{(2+n)\pi - \frac{t_B^2}{(n+2)\pi}\left(\frac{\nu l_x \delta}{2\pi I}\right)^2\left(\frac{n+1}{n}\right)} \tag{31}$$

Figure 4 is a plot of the required ω_x and I_x/I as a function of the burning time for the case in which n is 2.

The thrust misalignment angle δ is, of course, only known in a statistical sense. Figure 5 shows the variation of the errors in θ and γ as a function of δ. In this particular case, the system has been tuned such that the errors in pitch and yaw would be zero at the end of a 5.9 second burning period.

Pitch and yaw errors would be expected at the end of the burning period due to errors in the spin rate, the burning time, and in other parameters, such as I_x/I. Since the moments of inertia of the vehicle may be carefully adjusted prior to flight, only errors in θ and γ due to $\Delta\omega_x$ and Δt_B will be considered. Thus

$$\Delta\theta_{\Delta\omega_x} = \Delta A_{R_x}\left[\cos(R_x+\mu)\,t_B - 1\right] - A_{R_x}\sin(R_x+\mu)\,t_B\,\Delta(R_x+\mu) + \Delta A_{\omega_x}\left[1-\cos(\omega_x+\mu)\,t_B\right] + A_{\omega_x}\sin(\omega_x+\mu)\,t_B\,\Delta(\omega_x+\mu) \tag{32}$$

However, for a tuned system, $\Delta\theta_{\Delta\omega_x}$ is zero for small errors in ω_x. Similarly, $\Delta\theta_{\Delta t_B}$ is zero. In the case of the yaw angle, γ, the following errors would be expected:

$$\Delta\gamma_{\Delta\omega_x} \cong A_{R_x}\left(\frac{I_x}{I}\,\Delta\omega_x t_B\right) - A_{\omega_x}\,\Delta\omega_x\,t_B \tag{33}$$

and

$$\Delta\gamma_{\Delta t_B} \cong A_{R_x}\,(R_x+\mu)\,\Delta t_B - A_{\omega_x}\,(\omega_x+\mu)\,\Delta t_B \tag{34}$$

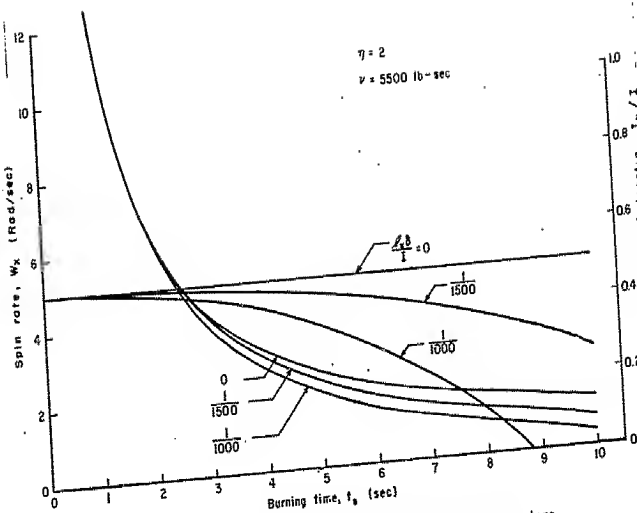

Fig. C-4—Required interrelationship of vehicle parameters which result in a period of oscillation of t_B

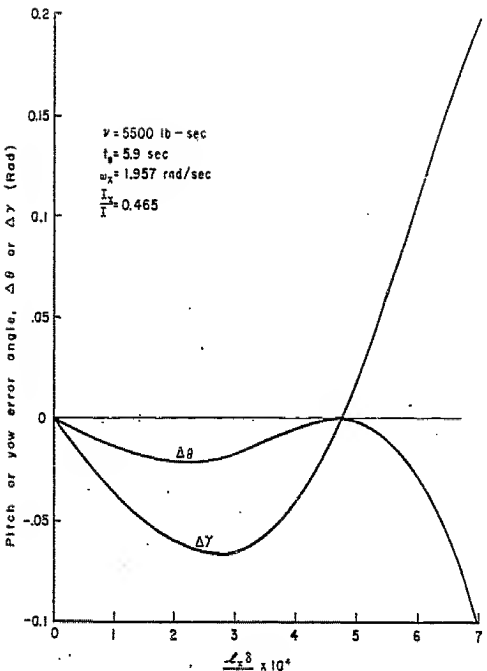

Fig. C-5—Pitch and yaw error angles at the end of burning as a function of the thrust misalignment errors

From the definitions of A_{R_x}, A_{ω_x} and μ upon page 8, it is apparent that $\Delta\gamma_{\Delta t_B}$ is also zero, while $\Delta\gamma_{\Delta\omega_x}$ is approximately zero.

After the burning period is over, Eq. (13) and Eq. (14) give the body rates, ω_y and ω_z. However, from the definition of R_z, and from Eqs. (26) and (27), it can be seen that $R_z\omega_x t_B$ is equal to 2π radians. Thus, ω_y and ω_z are zero for $t > t_B$.

Of course, the most direct approach in reducing the magnitudes of the forced errors in θ and γ is to increase ω_x. For large values of the spin rate, the amplitude constants, A_{R_x} and A_{ω_x}, approach zero, and it is not necessary to adjust the periods of the oscillations.

However, system operation dictates a spin rate of approximately 2 radians per second. Thus, unless the required increment in speed is, by design, kept small so that, in turn, the misalignment torque is small, the periods of oscillation should be tuned to ensure small errors after the propulsion period is over.

The next effect to be examined is that of residual aerodynamic forces. From consideration of Figs. 1 and 2 in conjunction with Eqs. (1) and (2), the following equations may be written:

$$\ddot{\alpha} + \dot{\theta}_V - \frac{\ell_{cp}}{I}\left(L_\alpha + D\alpha\right) + \left(\dot{\beta} + \dot{\gamma}_V\right)\left(\dot{\psi} - R_z\,\omega_x\right) = 0 \qquad (35)$$

$$\ddot{\beta} + \dot{\gamma}_V - \frac{\ell_{cp}}{I}\left(L_\beta + D\beta\right) - \left(\dot{\alpha} + \dot{\theta}_V\right)\left(\dot{\psi} - R_z\,\omega_x\right) = 0 \qquad (36)$$

where L_α is the lift force due to α, acting perpendicular to V,

L_β is the lift force due to β, acting perpendicular to V, and

D is the drag force acting along V. In obtaining Eqs. (35) and (36), all angles except ψ are assumed to be 'small angles.' Thus,

$$L_\alpha = \frac{1}{2} \rho V^2 A_{ref} \frac{\partial C_L}{\partial \alpha} \alpha \qquad (a)$$

$$L_\beta = \frac{1}{2} \rho V^2 A_{ref} \frac{\partial C_L}{\partial \beta} \beta \qquad (b) \quad (37)$$

$$D = \frac{1}{2} \rho V^2 A_{ref} C_D \qquad (c)$$

Upon adopting a circular orbit, and letting $\dot{V} = \omega_x$, Eq. (35) and Eq. (36) have the following form:

$$\ddot{\alpha} - \frac{\delta_{cp}}{I} \left(\frac{1}{2} \rho V^2 A_{ref} \right) \left(C_D + \frac{\partial C_L}{\partial \alpha} \right) \alpha + (\dot{\beta} R_x) = 0 \qquad (38)$$

$$\ddot{\beta} - \frac{\delta_{cp}}{I} \left(\frac{1}{2} \rho V^2 A_{ref} \right) \left(C_D + \frac{\partial C_L}{\partial \beta} \right) \beta - (\dot{\alpha} R_x) = - \frac{g_o r_E^2}{V r^2} R_x \qquad (39)$$

The solutions of Eqs. (38) and (39) may be readily obtained.

$$\alpha = \frac{+\frac{g_o r_E^2}{V r^2} R_x z_3}{z_1 (z_1^2 - z_3^2)} \sin z_1 t + \frac{\frac{g_o r_E^2}{V r^2} R_x z_1}{z_3 (z_1^2 - z_3^2)} \sin z_3 t \qquad (40)$$

$$\beta = - \frac{g_o r_E^2 R_x}{V r^2 \omega_n^2} - \frac{g_o r_E^2 R_x z_3^2}{V r^2 \omega_n^2 (z_1^2 - z_3^2)} \cos z_1 t + \frac{g_o r_E^2 R_x z_1^2 \cos z_3 t}{V r^2 \omega_n^2 (z_1^2 - z_3^2)} \qquad (41)$$

where

$$z_1 = \sqrt{\omega_n^2 + \frac{R_x^2}{4}} + \frac{R_x}{2}$$

$$z_3 = \sqrt{\omega_n^2 + \frac{R_x^2}{4}} - \frac{R_x}{2}$$

$$\omega_n^2 = - \frac{I_{cp}}{I} \left(\frac{1}{2} \rho V^2 A_{ref}\right) \left(C_D + \frac{\partial C_L}{\partial \alpha}\right)$$

As the aerodynamic effects become negligible, the parameter z_3 approaches zero, while z_1 approaches R_x. If the satellite has a two day operational capability, then the maximum value of t is of the order of 1.75×10^5 seconds. For the angle $z_3 t$ to remain small over this period of time, it is necessary that z_3 have a magnitude not greater than 10^{-6}. Thus

$$\omega_n^2 \leq 10^{-6} R_x \qquad (42)$$

Figure 6 is a plot of $\frac{I_{cp}}{I}$, the ratio of the static margin to the pitch-yaw moment of inertia, as a function of altitude with the restriction imposed by Eq. (42).

As a typical example, for an orbit altitude of 800,000 feet with R_x equal to one and with I equal to 20 slug-ft^2, the center of mass and the center of pressure may have a maximum separation of 0.575 inches to ensure that torques due to aerodynamic effects are negligible. With $z_3 t$ a small angle, Eq. (40) and Eq. (41) have the following form

$$\alpha = + \frac{g_o r_E^2}{V r^2} \left[t + \frac{\omega_n^2}{R_x^3} \sin R_x t \right] \qquad (43)$$

$$\beta = - \frac{g_o r_E^2}{V r^2} \frac{R_x}{\omega_n^2} \left[\frac{\omega_n^4}{R_x^4} \cos R_x t \right] \qquad (44)$$

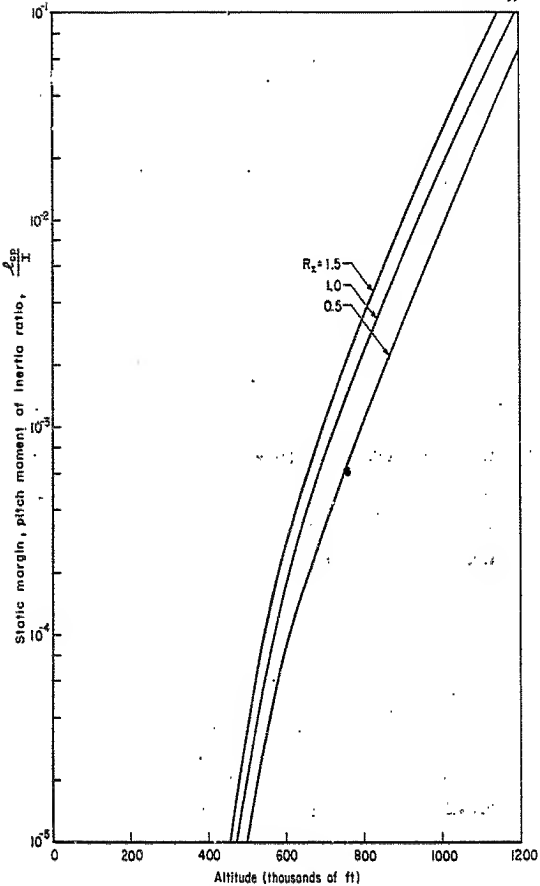

Fig. C-6—Permissible static margin as a function of altitude

Thus α is approximately equal to $\dot{\theta}_{ss}t$, while β is approximately zero, which is the result indicated by Eqs. (7) and (8) for the case of zero initial errors.

Disturbances which arise due to the motion of internal components may be minimized by the proper placement of such gear. As an example, any rotating machinery should be placed, if possible, with the axes of rotation coincident with the vehicle's longitudinal spin axis. The motion of such equipment will then cause perturbations in the spin rate, but will not exert moments which would result in a pitch or yaw motion.

If it were required the spin rate could be regulated by the use of a reaction wheel.

Other disturbances such as those due to meteor impact and magnetic field interactions may occur. However, the former event appears to be very unlikely,[1] while a preliminary examination of the latter effect indicates that for the vehicle under consideration, no significant errors should develop during a two day operational period.

Thus, the expressions for the total error in θ and γ are:

$$\Delta\theta = \pm \epsilon_\theta \pm 0.707\ \Delta A_{\theta,\gamma} \pm \Delta\theta_\delta \tag{45}$$

$$\Delta\gamma = \pm \epsilon_\gamma \pm 0.707\ \Delta A_{\theta,\gamma} \pm \Delta\gamma_\delta \pm \Delta\gamma_{\Delta\omega_x} \tag{46}$$

In order to evaluate the root sum squared values of $\Delta\theta$ and $\Delta\gamma$, the following values have been assumed:

$$\epsilon_\theta = \epsilon_\gamma = \pm 0.035 \text{ rad}$$

$$\epsilon_{\dot\theta} = \epsilon_{\dot\gamma} = \pm 0.035 \text{ rad/sec}$$

$$\omega_x = 1.957 \text{ rad/sec}$$

$$\Delta\omega_x = \pm 0.035 \text{ rad/sec}$$

$$\frac{I_x}{I} = 0.465$$

$$t_B = 5.9 \text{ secs}$$

The preceding values, in conjunction with Figs. 3 and 5 and Eqs. (45) and (46), yield:

$$\Delta\theta_{ras} = 0.087 \text{ rad}$$

$$\Delta\gamma_{ras} = 0.109 \text{ rad}$$

The primary source of rate disturbances is the initial residual error rates. Thus

$$\Delta\dot\theta = \Delta\dot\gamma = 0.049 \text{ rad/sec}$$

From the point of view of the operational requirements, the attitude stabilization of the vehicle poses no particular difficulties. The assumed performance of the orientation control system is within current capabilities.

(1.) Buchheim, R. W., 'Lunar Instrument Carrier--Attitude Stabilization,' The RAND Corporation, Research Memorandum RM-1730, June 4, 1956 (Unclassified).

Appendix D

GUIDANCE ACCURACY REQUIREMENTS

J. H. Huntzicker

The inaccuracies that may be tolerated in the ascent guidance system can be related to the design altitude, which is determined by a compromise of the desire for large scale and the requirement to keep aerodynamic forces negligible during the operation. One problem which should be resolved during the satellite test program is the determination of air density as a function of altitude; with these data a minimum operation altitude can be established.

For purposes of determining guidance tolerances a design altitude of 750,000 ft (142 mi) has been selected, with permissible variation being $\pm$250,000 ft (47.3 mi). At these altitudes aerodynamic effects are nominal. If the variation in altitude were to be considerably reduced the design altitude could, of course, be lowered.

This acceptable range of altitude (142 $\pm$47.3 mi) can be interpreted in terms of ascent guidance requirements in the following manner: The minimum or perigee altitude (h_p) and the maximum or apogee altitude (h_a) are uniquely determined by these conditions at the end of final, or third-stage, burning; the magnitude of the velocity (v_3), the direction of the velocity vector with respect to the horizontal (γ_3) and the altitude (h_3). They are related by the following equations:

$$r_a = \frac{v_3^2 r_3^2 \cos^2 \gamma_3}{\mu(1-e)} \qquad (1)$$

$$r_p = \frac{v_3^2 r_3^2 \cos^2 \gamma_3}{\mu(1+e)} \qquad (2)$$

where

$r_i = h_i + r_e$ (r_e = radius of the earth)

$\mu = g r_e^2$ (g = the gravitational constant)

and the orbital eccentricity e is defined by

$$e = \frac{r_a - r_p}{r_a + r_p}$$

and $$e = \left\{1 - (2 - v_3^2 r_3/\mu) \frac{v_3^2 r_3 \cos^2 \gamma_3}{\mu}\right\}^{1/2} \qquad (3)$$

Figure D-1 presents h_a and h_p as functions of Δv_3 for varying $\Delta \gamma_3$ where $\Delta v_3 = v_3 - v_c$ (v_c = circular velocity at 142 mi) and $\Delta \gamma_3 = \gamma_3$ (i.e., $\gamma = 0$ for a circular orbit). This figure does not include the effect of errors in the altitude of final burning (Δh_3). This effect can be approximated by

$$\frac{dh_a}{dh_3} = \frac{dh_p}{dh_3} = +2 \qquad (4)$$

Figure D-1 will yield a measure of the inaccuracies which are tolerable in the control of the ascent trajectory, but this only indirectly. For D-1 to be meaningful in terms of the performance required of the guidance equipment it is necessary to examine the flight path to determine where errors originate and how they propagate to the point of final thrust cut-off (Point 3).

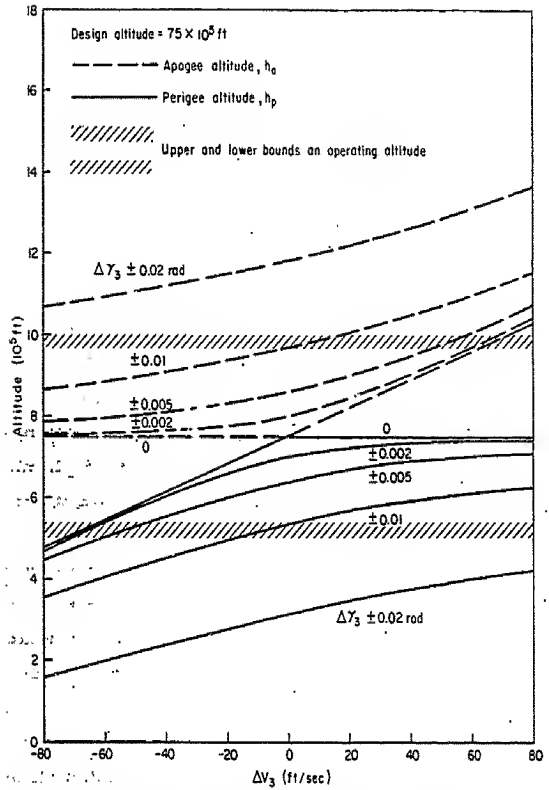

Fig. D-1—Apogee and perigee altitudes related to errors in the magnitude (ΔV_3) and direction ($\Delta \gamma_3$) of final burnout velocity

Figure D-2 illustrates a representative secent trajectory. At Point 1 second stage burn-out occurs, followed by orientation and spinning of the third stage. A long coasting period (about 4800 n mi) takes the vehicle from Point 1 to Point 2 where third-stage burning occurs. Point 3 is the point of final burn-out and hence the initiation of orbiting.

Inaccuracies in guidance prior to Point 1 will result in errors in altitude, velocity, and direction at Point 1. Each of these errors contributes to errors in all three quantities at Point 3. Errors are also introduced by inaccuracy in the control of the magnitude and direction of the velocity increment added between Points 2 and 3. Due to the small amount of velocity added in the third stage (approximately 300 to 500 ft/sec) the effects of these errors should also be small (e.g., if the velocity varied by $\pm$ 2 per cent and the direction by $\pm$ 5 degrees the resultant errors in final cut-off conditions are $\pm$ 10 ft/sec and $\pm$ 1.7 mils, which, if added with zero correlation to the errors originating at Point 1, will be negligible.)

The assumption was made that final burning occurs at a constant range angle measured from Point 1. If final burning were controlled with a preset clock, further errors would be introduced by inaccuracies in the clock and by variations in the time required to reach the desired range angle. The latter introduces an error in range angle of less than 10 miles. Comparable accuracy in the time base would require a clock accurate to about 0.1 per cent (~80 sec/day). These effects will be insignificant relative to those caused by errors in second-stage cut-off conditions.

On the basis of the preceding considerations the remainder of this study was restricted to an examination of the propagation of errors from

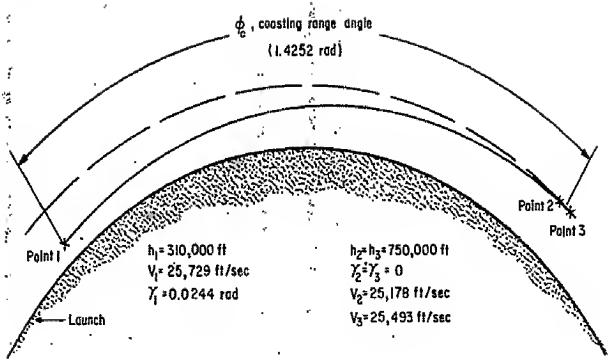

Fig. D-2 — Representative oscent trojectory

Point 1 to Point 3 (nearly identical in space to Point 2). During the coasting from Point 1 to Point 2 the vehicle follows an ellipse described by

$$r = \frac{v_1^2 r_1^2 \cos^2 \gamma_1}{\mu(1-e\cos\phi)} \tag{5}$$

where ϕ is the range angle measured from the apogee of the ellipse and

$$v_1 = v_{d1} + \Delta v_1$$

$$r_1 = r_{d1} + \Delta r_1$$

$$\gamma_1 = \gamma_{d1} + \Delta\gamma_1$$

The symbols v_{d1}, r_{d1} and γ_{d1} are the design conditions at Point 1 as indicated on Fig. D-2. The values Δv_3, Δr_3 and $\Delta\gamma_3$ are calculated at a point down-range ϕ_c radians (ϕ_c is the design coasting range angle - see Fig. D-2); ϕ_3 will be equal to $\phi_1 + \phi_c$ (ϕ_1 being negative inasmuch as the apogee is down-range from Point 1).

In addition to Eqs. (3) and (4) the following are used:

$$\frac{2\mu}{r} - v^2 = \frac{2\mu}{r_1} - v_1^2 \tag{6}$$

$$\tan\gamma = \frac{-e\sin\phi}{1-e\cos\phi} \tag{7}$$

The final errors are then

$$\Delta v_3 = v_2 - v_{d2} \tag{8}$$

$$\Delta r_3 = r_2 - r_{d2} \tag{9}$$

$$\Delta\gamma_3 = \gamma_2 \tag{10}$$

These were calculated for all combinations of a range of values of Δv_1, Δr_1 and $\Delta\gamma_1$. Representative results are plotted as Figs. D-3, D-4

and D-5. As can be seen, the relationships are quite linear within the range of interest and can be approximated by

$$\Delta v_3 = -2.5 \times 10^{4} \Delta\gamma_1' - 0.75\,\Delta v_1 - 10^{-3} \Delta r_1 \qquad (11)$$

$$\Delta r_3 = 2.1 \times 10^{7}\, \Delta\gamma_1' + 1.5 \times 10^{3} \Delta v_1 + 2\Delta r_1 \qquad (12)$$

$$\Delta\gamma_3' = 0.1\, \Delta\gamma_1' + 7.5 \times 10^{-5}\, \Delta v_1 - 5 \times 10^{-8} \Delta r_1 \qquad (13)$$

A marked negative correlation exists between Δv_3 and Δr_3, the net effect being to limit the variation of h_a and h_p of the final orbit (see Fig. D-1). This is further demonstrated by the inclusion of Δv^* on Figs. D-3, D-4 and D-5, where Δv^* is the velocity error defined with respect to the actual altitude at Point 3 rather than the design altitude. The value of Δv^* is in general only a fraction of Δv_3.

Based on the foregoing we can stipulate the approximate accuracy required of the first- and second-stage guidance equipment. In order to establish an orbit which will remain within altitude limitations of 142 $\pm$ 47 mi we could tolerate probable errors in velocity of as much as $\pm$50 to $\pm$75 ft/sec and probable errors in angle of up to $\pm$4 to $\pm$6 mils.

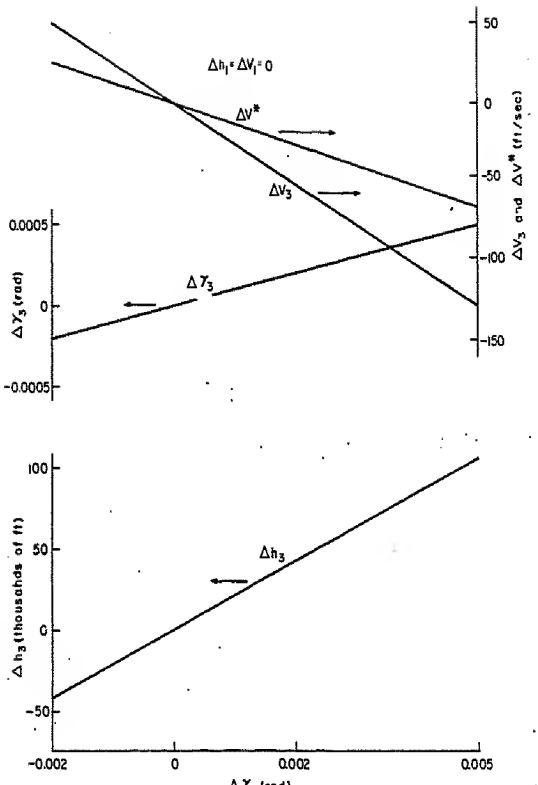

Fig. D-3— Errors in altitude (Δh), velocity (ΔV), and flight path angle ($\Delta \gamma$) at point 3 due to errors in flight path angle at point 1 ($\Delta \gamma_1$)

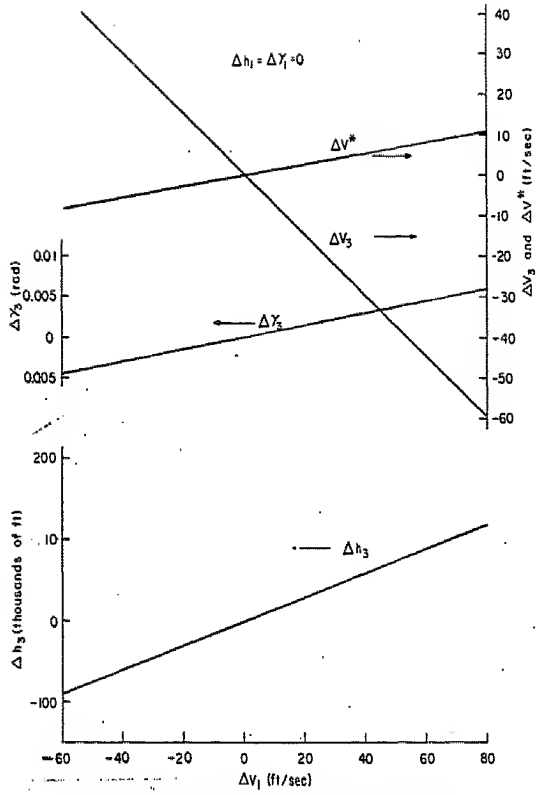

Fig. D-4— Errors at point 3 (ΔV, Δh, ΔV^*, and $\Delta \gamma_3$) caused by errors in velocity at point 1 (ΔV_1)

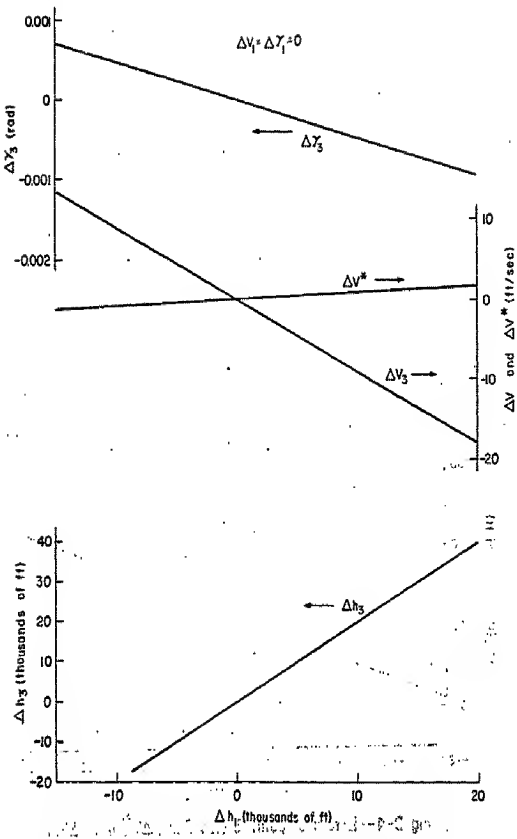

Fig. D-5 — Errors at point 3 (ΔV, Δh, ΔV^*, and $\Delta \gamma_3$) caused by errors in altitude of point 1 (ΔV_1)

Appendix E

FLIGHT MECHANICS

H. A. Lieske

The main features of the orbit of this proposed system are the inclination of the orbit and the spatial orientation of the satellite vehicle: the orbit is to be in a plane passing through the poles, and the satellite is to be oriented so that its roll axis is horizontal at a latitude of 55 deg — that is, the roll axis is at an angle of 35 deg relative to the equatorial plane. A polar orbit requires that the satellite be launched in a southerly direction from Camp Cooke (latitude 34.5 deg North), and that the roll axis of the satellite be oriented so that it is horizontal at a latitude of 55 deg South. If the final orbital velocity increment is to be added at 55 deg latitude south, the total ascent is approximately 5400 n mi. That is, this satellite ascent path is equivalent to the first half of a shallow ballistic missile trajectory of about 10,000 n mi total range. This ascent path will require the maximum performance capability from the booster combination. An alternate method of establishing the orbit with the correct satellite orientation will be discussed later.

The launching vehicle for the satellite consists of a two-stage booster combination – the Thor and the second stage of Vanguard – plus a small solid propellant rocket of the Vanguard third-stage type to give the final orbital velocity increment. The booster stages are described in Appendix F. The vehicle parameters pertinent to the performance study are repeated in Table 1.

Table 1

VEHICLE PERFORMANCE PARAMETERS*

Thor		Vanguard II	
W_{E_1}	= 13,880 lb	W_E	= 1430 lb
W_{prop_1}	= 97,030 lb	W_{prop}	= 3320 lb
I_o	= 245 sec (sea level)	I	= 278 sec (vacuum)
T	= 150,000 lb	T	= 7500 lb
t_B	= 158.5 sec	t_B	= 123 sec

Final Stage (solid rocket)

I = 245 sec (vacuum)

V^* = 0.750

*These parameters were used in the trajectory analysis.

The burnout velocity of the booster combination was approximated by use of the theoretical velocity potential of each stage minus the approximate values of the velocity losses due to drag and gravity. The velocity loss due to gravity during the Thor powered stage, flown on a gravity-turn path, is shown in Fig. E-1 as a function of the first-stage-burnout path angle. The velocity loss due to drag for a nominal configuration is also included. The second-stage gravity loss is given in Fig. E-2, also for a gravity-turn path. The curve of first-stage-burnout path angle is included to relate the two figures.

An average specific impulse ratio $\bar{I}/I_0 = 1.13$ was used for the first stage. The second stage operates at altitudes above 200,000 ft so that its drag deceleration will be small and is neglected in this analysis. The second stage specific impulse will be constant at the vacuum value of 278 sec.

The approximate burnout altitudes of the first and second stages are given in Fig. E-3 as functions of second-stage path angle. The first- and second-stage burnout ranges are approximately 90 and 450 n mi respectively, for trajectories which are nearly horizontal at second-stage burnout.

The final burnout velocity, at a given path angle, is given by

$$V_{B_2} = -g\bar{I}\log_e(1 - v_1) - gI_2\log_e(1 - v_2) - \Delta V_{D_1} - \Delta V_{g_1} - \Delta V_{g_2}$$

where the propellant-gross weight ratios v_1 and v_2 are determined from the assumed second-stage payload weight and the data given in Table 1.

The second-stage payload weight is given by

$$W_{pay_2} = \frac{W_{orb}}{1 - v/v^*} + 25$$

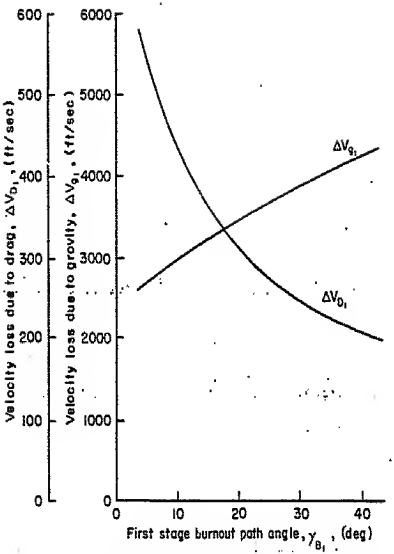

Fig. E-1 — Velocity loss during first stoge

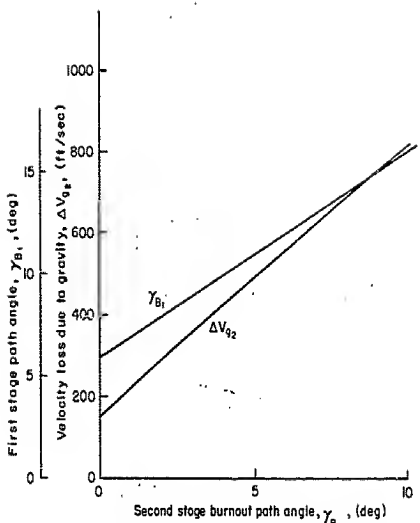

Fig E-2—Velocity loss during second stage

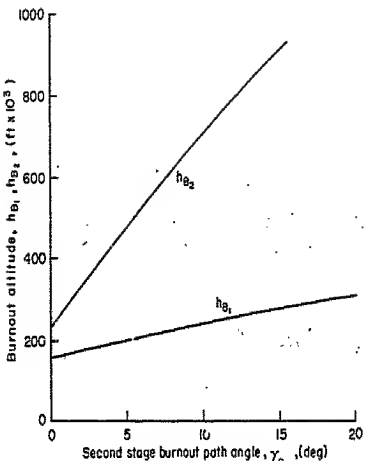

Fig. E-3—Burnout altitudes

with a propellant – total motor weight ratio v^* of approximately 0.75 (see Appendix F), and the required v value computed from the orbital velocity increment using a specific impulse I_3 = 245 sec.

The ascent trajectory for an orbiting weight of 300 lb launched from Camp Cooke directly into the orbit at 55 deg south latitude is shown in Fig. E-4. (This ascent trajectory was computed for a circular orbit at an altitude of about 180 stat mi.) The total booster velocity potential, with a second-stage payload weight of 350 lb, is 29,350 ft/sec which is decreased to a burnout velocity of 25,700 ft/sec by the losses due to drag and gravity on this shallow trajectory. The second-stage-burnout path angle is 2 deg at an altitude of 335,000 ft, resulting in an eccentricity of about 0.035 for the free-flight ascent ellipse. The circular orbit velocity increment required for this trajectory is only 450 ft/sec, which is typical of a long range satellite ascent trajectory. The solid rocket motor for this orbital velocity increment will weigh about 25 lb. The total required velocity potential of the three powered stages is 29,800 ft/sec for this ascent trajectory.

The effect of total ascent range on the allowable orbiting weight is shown in Fig. E-5. It can be seen that the allowable orbiting weight for this vehicle combination could be about 400 lb, or an increase of about 30 percent, if the ascent range were about 2700 n mi, or half the range required for launching the satellite from Camp Cooke and entering the orbit at a latitude of 55 deg South.

The relative velocity contributions of the booster combination and of the final stage will vary as the ascent range is changed. As the ascent range is decreased, the required orbital velocity increment is increased while the booster velocity increment is decreased. The net result is an

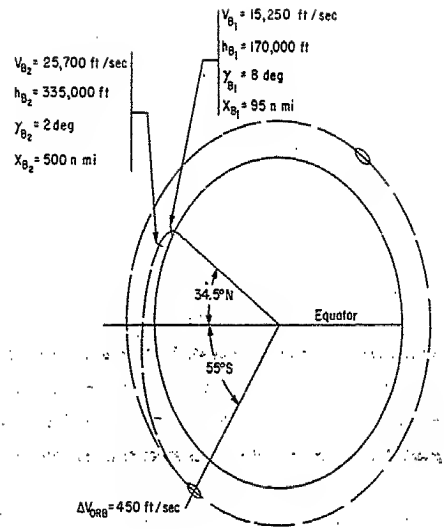

Fig. E-4— Typical descent from Comp Cooke

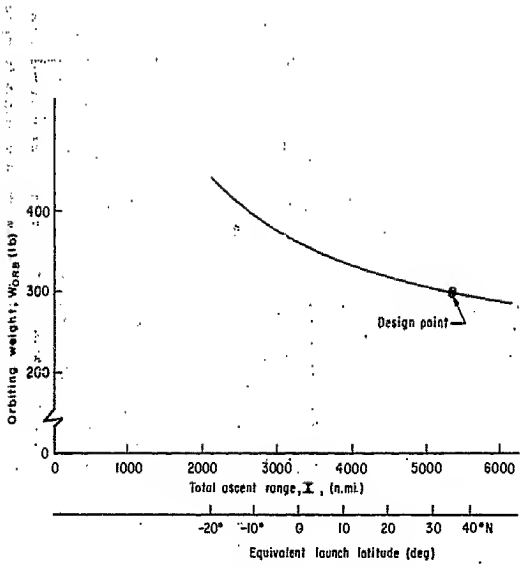

Fig. E-5— Orbiting weight vs ascent range

increase in the allowable orbiting weight as the ascent range is reduced to a more nearly optimum value for this booster combination.

The lower horizontal scale of Fig. E-5 indicates the corresponding launch latitude for orbit entry at 55 deg South. For example, if the launch site were at a latitude of approximately 10 deg North (Panama), the allowable orbiting weight for this booster combination would be increased by about 10 per cent. Alternately, if the orbiting weight were fixed at a value of 300 lb, a small performance margin would be available.

Another possible scheme of establishing the satellite in an orbit with the required vehicle orientation (horizontal at 55 deg South) is sketched in Fig. E-6. The trajectory parameters at second-stage burnout are such as to lead to a free-flight ellipse which has an apogee altitude somewhat higher than the required orbital altitude at a shorter distance from the launch site. After second-stage burnout, the satellite vehicle is oriented correctly (roll axis at 35 deg relative to the equator) and spun to the required roll rate. When the vehicle coasts up to the required orbital altitude at an intermediate latitude, l_1, the third stage, which is oriented as mentioned above, adds the appropriate velocity increment to the vehicle's velocity in the ellipse so that the resultant velocity is directed horizontally at that point with a magnitude equal to the required circular orbital velocity. The final velocity increment required for this method of orbit injection will be somewhat larger than the value required for injection at 55 deg South (Fig. E-4), so that the final-stage gross weight will be increased slightly. The variation of orbiting weight with range to apogee shown in Fig. E-5, however, is such that the required weight increase may be compensated for.

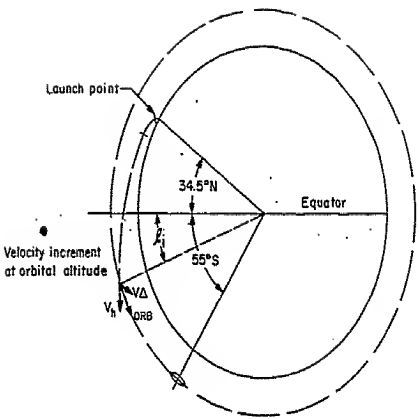

Fig. E-6—Alternate satellite ascent

Appendix F

VEHICLE DESIGN SUMMARY

E. C. Heffern

FIRST-STAGE BOOSTER

Thor (WS-315) IRBM is used to provide the initial rocket-powered boost for the proposed satellite. Based on a preliminary review of the Thor airframe and its major components and systems, it appears that an upper stage, or stages, weighing 5000 lb could be placed on the Thor without modification to the basic airframe and its primary components. The estimates presented in this report are intended to outline the more basic considerations associated with the use of the Thor as a first-stage satellite booster, and are not intended to reflect a complete analysis.

For the trajectory analysis presented in Appendix E, a weight summary of the Thor missile is given in Table 1. These data are based on information contained in Refs. 1 and 2.

Table 1

WEIGHT SUMMARY - THOR MISSILE (lb)

Structures Group	3060	
Propulsion Group	2380	
Guidance and Control Group*	1565	
Separation System	30	
Electrical System*	200	
Dry missile - less upper stages		7235
Unusable Propellants	1525	
Pressurization Gases	372	
Burn-out Weight - less upper stages		9132
Usable Propellants	97,030	
Take-off Weight - less upper stages		106,162

*Modified weights - see discussion below.

The modified guidance and electrical system weights are due to the omission of the ACSP guidance unit and a portion of the vernier system for the satellite mission. Elimination of the guidance unit reflects a weight reduction in the electrical power system, as well as in the guidance system, because of reduced power requirements. (It is assumed that the required electrical power is obtained from the same type battery-inverter power source used in the early Thor missile.) Since vernier rockets will be required only for control during the main-rocket boost in this application, the vernier propellant tanks may be omitted. The allowance for unused propellants shown in the table includes a 1 per cent reserve for propellant utilization errors.

Although the axial loads resulting from the 5000-lb upper-stage load (the design re-entry-body weight is 3500 lb) are estimated to be within the load-carrying capability of the Thor airframe, the increased length of the upper stages may result in a larger airload and larger bending loads, which may require localized stiffening in the guidance section and in the section between the tanks. Because of the differences in the diameter of the re-entry adaptor ring and the body diameter of the upper stage, it may be desirable to consider a modified nose, or guidance, section for the Thor missile. The actual design of this section would, of course, be determined by the actual design choice of the upper stage. If the second stage of the Vanguard system is used on the Thor booster, this guidance section may be modified as shown in Fig. F-1.

SECOND-STAGE BOOSTER

The second-stage of the Vanguard vehicle is utilized as an example

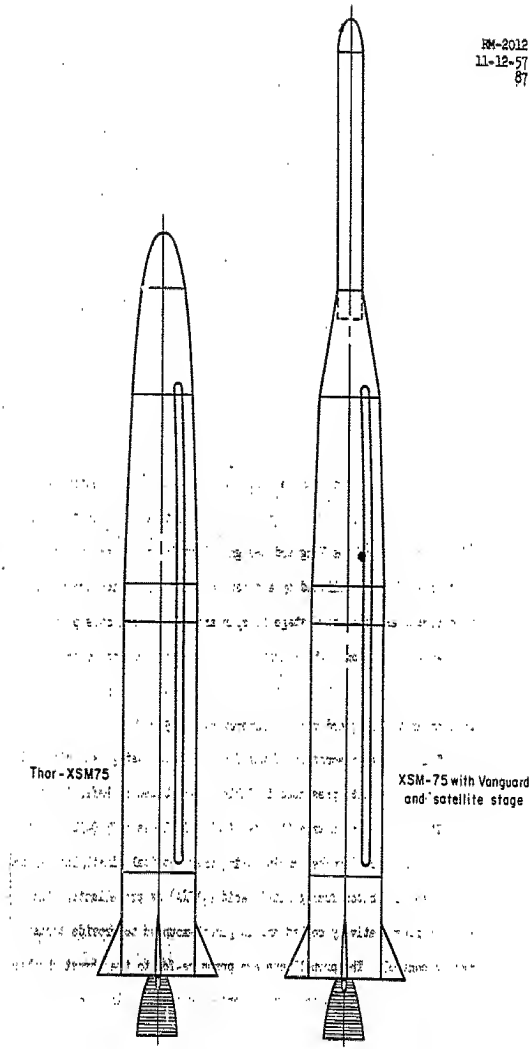

Fig. F-1—General arrangement

of the type of vehicle, and the performance required, for adaptation to the Thor airframe for satellite missions. Although other missile components could be included for this application, it is believed that the Vanguard second-stage could be available at an earlier date and would have a greater flexibility than other components; for example, a modified Sergeant-type solid-propellant booster with a special control system added for vehicle orientation after burn-out.

The Vanguard second stage consists of a propulsion package manufactured by the Aerojet-General Corporation and assembled into a complete second stage by the Martin Company with the addition of the guidance (autopilot) and control components. The basic ascent trajectory and sequence of operations for the proposed satellite are predicated on many of the features of the Vanguard design. That is, there are two phases of powered flight, followed by a coast period during which the missile is oriented and the third stage is spun around its roll axis prior to third-stage ignition. The weight of the satellite package discussed in the following section, 300 lb, is less than the weight carried by this section in the Vanguard vehicle (approximately 500 lb).

This summary discussion of the Vanguard second-stage vehicle, and the performance data presented in Table 2, are based on Refs. 3 and 4.

The propulsion package (Aerojet AJ-10) includes a 7500-lb thrust (vacuum conditions) rocket engine using unsymmetrical dimethylhydrazine (UDMH) and inhibited fuming nitric acid (WIFNA) as propellants. The engine is regeneratively cooled and is gimbal-mounted to provide thrust vector control. The propellants are pressure-fed to the thrust chamber by the pressurizing gas (helium augmented by a solid gas generator). The

Table 2

VANGUARD SECOND STAGE

Weight Data

Structure	150
Powerplant (including tanks)	450
Controls and guidance	270
Electrical system	150
Dry missile weight (less upper stage)	1020
Residuals	60
Burn-out weight (less upper stage)	1080
Usable Propellants	3320
Gross stage weight	4400

Performance Data (vacuum conditions)

Thrust	7500 lb
Specific impulse	278 sec

pressurization system (helium tank) is located between the propellant tanks. After main-stage burn-out, the residual pressurizing gases are used in the control jets for orientation control during the coasting phase of the trajectory.

The second-stage structure includes an aft skirt, tank section, and the forward instrument and housing section. The aft section is constructed of a magnesium alloy, while the tank section (with the integral pressurization sphere) is heat-treated stainless steel. The forward instrument and housing section are of a magnesium-thorium alloy. This section houses the guidance equipment, the spin assembly, and the third-stage solid propellant rocket. The satellite (orbiting stage) is attached to this section as shown in Fig. F-2.

THIRD-STAGE ROCKET

The long-range ascent path for this type of satellite requires the addition of only a small velocity increment (about 450 ft/sec) to place the vehicle in orbit. A shorter ascent path would permit a heavier payload to be carried, but the increased ΔV required for the orbit would call for a larger unguided solid-propellant rocket than is stipulated here, with attendant undesirable increases in angular and velocity errors (see Appendix E). Uncertainties in the total impulse of the solid rocket (about 1 per cent) could be expected to vary the actual velocity increment by 1 per cent or about 5 ft/sec for the selected trajectory, which can easily be tolerated.

The design of the solid third-stage rocket is based on a shortened Scale-Sergeant case and grain using Vanguard third-stage propellants, which gives 245 sec specific impulse at altitude. The propellant weight

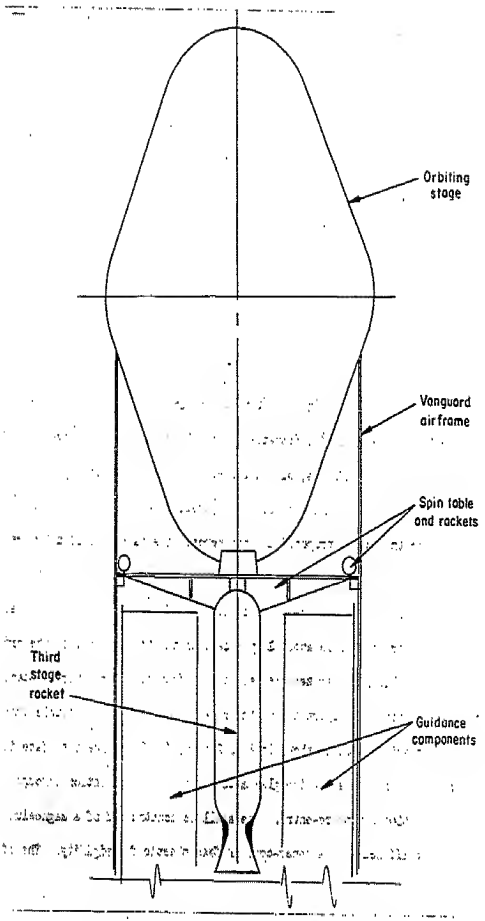

Fig. F-2- Satellite and third stage rocket

of 20 lb with an inert weight of 6 lb will give the required velocity increment of 450 ft/sec.

SATELLITE STAGE

For this discussion, the satellite stage is divided into three major components: the payload installation, the recovery system, and the structure. The payload equipment...is considered to be packaged in a short cylindrical section (35 inches in diameter, 6 inches in length).... A list of the components and the estimated weights are included in Table 3.

The recovery system includes the tracking and recovery beacon, and the retro-rocket which is the heaviest single component in the satellite. For simplicity it is suggested that the entire satellite be recovered. As larger payload is incorporated, it may be desirable to recover only individual packages, allowing a greater percentage of the satellite to be utilized for useful payload.

For the design proposed in this report, the retro-rocket delivers approximately 1500 ft/sec velocity increment to initiate descent from orbit. The Sacle-Sergeant motor is adequate for this application. Weight of the retro-rocket is about 22 per cent of the total weight of the orbiting stage. Table 4 summarizes the weight breakdown of the recovery system.

The basic configuration of the satellite is a modified double cone with spherical ends as shown in Fig. 2 on p. 6. The forward surface is covered with a plastic-fiberglas material for heat protection through vaporization during re-entry. The shell is constructed of a magnesium alloy stiffened with a honey-comb or foam plastic for rigidity. The aft

Table 3

PAYLOAD INSTALLATION WEIGHTS (lb)

Payload System		51.5
Altitude Sensor		8.5
	Window	0.5
	Sun sensor	1.
	Battery	3.0
	Clock	1.0
	Misc.	
Container		20
	Metal parts	15
	Environment	5
Total Installation Weight		80

Table 4

RECOVERY SYSTEM WEIGHTS (lb)

Retro-rocket	60
Propellants	51
Inert parts	9
Tracking beacon	16
Beacon	
Transponder	
Battery	
Antenna & cable	
Recovery beacon	9
Beacon	
Battery	
Antenna & cable	
Total installation weight	85

portion of the shell structure is covered with a thin plastic coating for heat protection. A summary of the structural weights is given in Table 5.

--

Table 5

STRUCTURE WEIGHT SUMMARY (lb)

Metal skin	15
Heat shield	65
Aft plastic covering	10
Plastic foam	40
Total structure weight	130

REFERENCES TO APPENDIX F

1. Douglas Aircraft Company, Report SM-27156, Thor WS-315A Technical Report, January-December 1956 (Secret).

2. Douglas Aircraft Company, Report SM-27034, Thor WS-315A Weight Status Report, December 15, 1956 (Secret).

3. U.S. Naval Research Laboratory, Design Specifications for Vanguard Launching Vehicle, NRL Spec. No. 4100-1, revised 29 March 1956 (Confidential).

4. U.S. Naval Research Laboratory, Project Vanguard Report of Progress, Status, and Plans, 1 June 1957 (Confidential).

Appendix G

TRACKING

R. T. Gebler

Tracking the satellite will be required to establish an orbit sufficiently accurate for coordination of data, for triggering the retro-rocket at the desired time for descent, and for establishing the descent path to facilitate impact location. Because of the near-polar orbit, location of tracking stations at high altitudes will be favored. The required number and location of trackers will be dictated partly by the guidance accuracy on which one can depend.

Since tracking accuracy deteriorates at low elevation angles, it is highly important that the satellite pass within a range which permits sufficient tracking data to be obtained at elevation angles greater than 20°. For a nominal 150-mile (statute) height, this requires that the satellite pass within 5° of the station (measured on a great circle path), or within 345 miles ground range. To ensure against guidance inaccuracy in launching, it is suggested that two or three trackers be used in an arrangement which generally places them with a 200 mile east-west separation. For a launching from Camp Cook and recovery in the Pacific, this would indicate Alaska as a favored location for these trackers, from which the descent would be commanded and the impact point predicted. Three such trackers located at a reasonable high latitude in the eastern part of the United States or Canada would be required to track an early pass for orbit prediction.

Tracking data would be in the form of two angles and a range to give position fixes necessary for orbit prediction. A minimum of two positions

and the corresponding time are required. Additional tracking data would necessarily be used in reducing the effect of noise errors. The use of range information relaxes considerably the requirement for angular accuracy. To obtain range, a transponder in the satellite is required. This, however, is consistent with the requirement for a command receiver in the satellite for firing the retro-rocket. For a CW system, modulation of a command transmitter at the tracker and remodulation in the satellite in a manner similar to that used by Azusa for range measurement is a feasible scheme.

The frequencies used would be nominally 500 mc for the satellite transmitter and 200 mc for the ground-command transmitter. Since circular polarization is required, the satellite antenna would be a turnstile or helical design so located that the inertial orientation of the vehicle will point the axis of the antenna toward the tracker to within at least 60°. Amplitude modulation of the output stage of the satellite transmitter, which will have a crystal-controlled master oscillator, will permit tracking in angle by either an interferometer-type system or a conical scanning system. It would permit range measurement to be made by phase comparison of the modulation frequency which is transmitted one way on a nominal 200-mc carrier and back on a nominal 500-mc carrier.

For a satellite at 150 (statute) miles height on a circular orbit, a velocity increment of 1500 ft per sec delivered along the longitudinal axis when the vehicle is at 65° N. Lat. (over Alaska) will cause a descent to about 200,000 ft altitude in about 6 minutes with impact about 3.5 minutes later. If commanded at 65° N. Lat. the impact will occur at about 32° N. Lat. Generally, it would be preferred that the satellite pass near

the zenith with respect to the tracker since this gives the maximum amount of useful tracking data, but conventional radar trackers are not gimballed to permit tracking through the zenith.

Preliminary estimates indicate that a tracker which can measure angles to about 0.1 mil and range to about 0.1 mi of systematic error, will permit prediction of the impact point to about 3 n mi if the tracking is accomplished after the descent has been commanded. Angle information good to about 0.1 mil (systematic error) can be obtained from either a conical-scan system or an interferometer type.

A CW-type transponder can be designed with smaller space and weight requirement in the vehicle than a pulse system with the required performance. It is estimated that a pulse-type transponder can be adapted from an existing design and will weigh about 15 pounds with power supply. A CW-type could be built to weigh about 10 pounds with power supply.

Since early availability is of paramount importance, one should probably consider adapting an existing tracking radar such as the FPS-16, or Nike missile-tracking radar to do the job. This would require modification of the range circuits, at least in the Nike. If one considers the use of shipborne radars and probably reduced accuracy in prediction, the SPG-49 is a good possibility.

For a recovery beacon it is proposed that a spring-ejected whip antenna be extended vertically through the satellite skin after impact. The antenna will be excited by a 50 mc oscillator designed to radiate about 0.25 watt. The signal strength at 50 miles would be about 35 μv/meter which should be adequate for airborne direction finding. The estimated weight for this design, for a 3-day operation, totals about 5 pounds for the transmitter, antenna, and batteries.

Appendix H

RE-ENTRY AND RECOVERY

C. Gazley, Jr.

DEPARTURE FROM ORBIT

Descent from the orbit is achieved by the command firing of a braking rocket as described in Ref. 1. Since the vehicle's orientation is conditioned by [geometry], and because of the relative positions of that area and the desired recovery area, the braking rocket is fired forward and upward. This results in a downward and backward velocity impulse superimposed on the orbital velocity. The resulting velocity vector is oriented downward at an angle γ with the local horizontal (Fig. H-1). The vehicle is now effectively in a ballistic trajectory comparable to the 'low-angle' (i.e., lower than optimum) path of a long-range ballistic missile.

For the desired range of about 2,000 n mi and an impulse angle $\theta = 110\text{-}125^{\circ}$, a velocity impulse $\Delta V = 1{,}500\text{-}2{,}000$ ft/second is required. This yields a resultant velocity $V_R \approx 24{,}800$ ft/second and a path angle $\gamma = 3\text{-}4^{\circ}$. Descent from this point follows a 'vacuum' path down to an altitude of about 250,000 ft. Below this altitude, atmospheric drag effects increase and ultimately predominate over gravitational influences.* Vacuum ranges are shown in Fig. H-3 as a function of the magnitude and angle of the velocity increment. Descent from the orbital altitude to 250,000 ft is accompanied by a velocity increase to 25,500 ft/second and an angle

*The altitude region where drag becomes important depends, of course, on the drag-mass characteristics of the body.

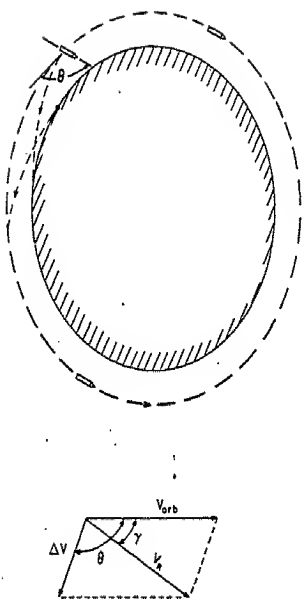

Fig. H-1—Vehicle orientation in orbit and at time of velocity increment

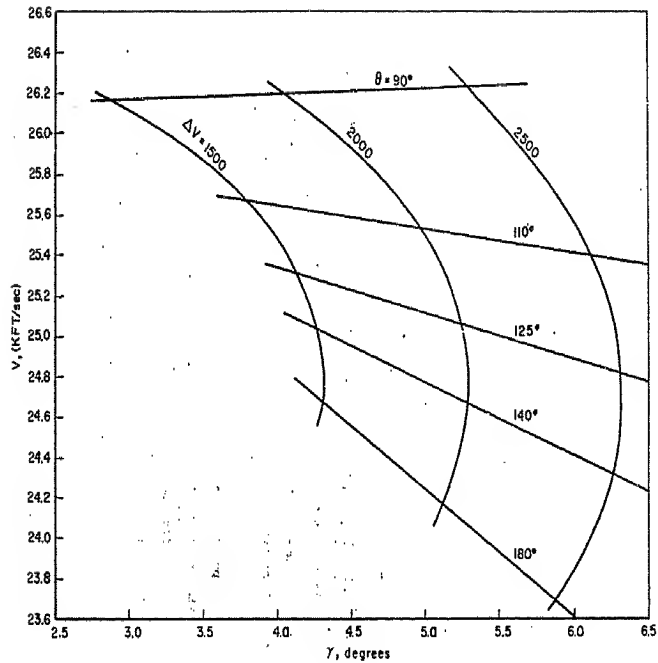

Fig. H-2—Conditions of altitude of 250,000 ft as a function of magnitude and angle of velocity increment

Circular orbit = 150 statute miles

increase to $\gamma = 4^{\circ}$ or 5°. Conditions at this altitude are shown in Fig. H-2 as functions of the impulse characteristics.

Radio observation of the vehicle immediately after the beginning of descent establishes a predicted vacuum path. This, together with estimated atmospheric effects, enables a prediction of an approximate impact area. The problem is similar to that described previously for the recovery of a satellite through natural decay of the orbit.[2] In that case, the predicted impact area was a narrow strip, a few miles wide and several hundred miles long. In the present case, the steeper descent results in a smaller uncertainty in range error. Final recovery is accomplished by overflight search. This, of course, requires operation of the radio beacon after the water impact.

ATMOSPHERIC DRAG AND DECELERATION

The effect of the earth's atmosphere on the vehicle's path and velocity is dependent both on the approach path and on the vehicle's mass-drag characteristics. For even a rather shallow entry angle (say 5° or more), the path in the atmosphere is essentially linear - at least until after appreciable deceleration and heating have occurred. For this type of path, an approximate analysis[3] is sufficiently accurate for estimation of deceleration and heating. By this analysis, the velocity altitude variation is given by:

$$\frac{u}{u_1} = e^{-\frac{C_D A_c}{W \sin \gamma} \frac{\rho_{SL}}{2\pi} \sigma} \qquad (1)$$

The velocity-altitude variation, as given by this equation, is shown in Fig. H-3 for several values of the drag-mass parameter, $C_D A_c / W \sin \theta$. It is seen that similar curves result, with relative displacements for various values of the drag-mass parameter. The maximum deceleration occurs when the velocity has been reduced to about 61 per cent of the initial value. The maximum deceleration is independent of the vehicle's size, shape, and mass and is dependent only on the initial velocity and on the entry angle. For the present case, the maximum deceleration amounts to about 20 g's. The altitude of maximum deceleration is dependent on the entry angle as well as on the drag-mass characteristics of the body.

As in any preliminary design, the tentative choice of parameters involves a cyclic process in which considerations of structure, heating, recovery, etc., all contribute to the final choice. Although the reasons for choosing various phases of the vehicle design will be developed in this Appendix, it is necessary for discussion purposes to describe that design here. The vehicle is essentially an ellipsoid with a maximum diameter of about 3 ft. While its orbital weight is 300 lb, about 50 lb (of propellant) is used to initiate descent from orbit, so that the weight at atmospheric entry is about 250 lb. This results in a drag-mass parameter, $C_D A_c / W \sin \gamma = 0.153$ sq ft/lb, which yields the velocity-altitude variation shown by the dotted line in Fig. H-4. A maximum deceleration of about 20 g's occurs at 110,000 ft altitude. Choice of the weight stemmed from booster capabilities and desired payload. Size and shape evolved from considerations of packaging and of heating and recovery. The payload, radio beacon, antenna, batteries, etc., are arranged to preserve entry stability and permit recovery.

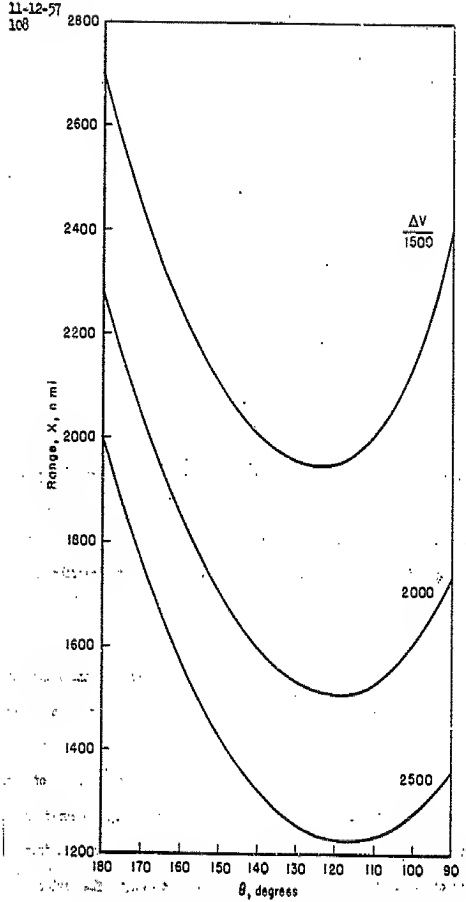

Fig. H-3—Vacuum descent range as a function of magnitude and angle of velocity increment

Circular orbit = 150 statute miles

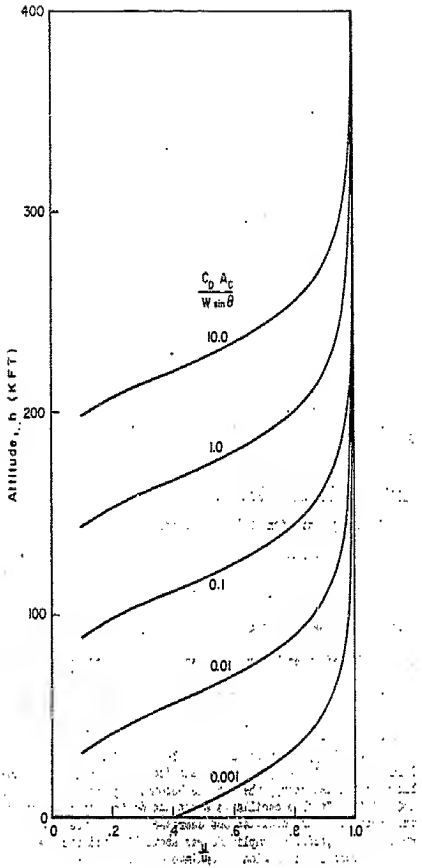

Fig.H-4—Velocity variation with altitude for atmospheric entry

As previously noted, the orientation of the vehicle is controlled by a moderate spin rate so that the vehicle is properly oriented .... The original orientation will be approximately preserved during the first part of the return trajectory, so that initial atmospheric entry will be rear-end first. By displacing the center of gravity toward the front of the body, aerodynamic forces can be made to re-orient the body. The design, of course, should be such that the re-orientation is completed before heating is appreciable.*

Ultimately the body falls vertically at terminal velocity:

$$u = \frac{1}{\sqrt{\frac{C_D A}{W} c \frac{\rho_{SL}}{2g} \sigma}} \qquad (2)$$

which results in an impact velocity of about 400 ft/second for the body described.

RE-ENTRY HEATING AND SURFACE PROTECTION

During penetration of the atmosphere, a vehicle's kinetic energy is converted into thermal energy of the surrounding air. Some of this thermal energy is transferred to the body as heat. The rate of this transfer varies during descent both with air density and vehicle velocity. Heat is transferred by both convection and radiation from the hot gas 'cap' over the front of the body to the body's surface. The rates of both con-

*A similar problem occurred in the case of the recovery of a circumlunar vehicle.[4] A dynamic analysis indicated that, for an essentially backward initial entry, the vehicle becomes righted at an altitude of about 250,000 ft. It then oscillates about the desired orientation; as the altitude decreases, the oscillations decrease in magnitude and increase in frequency. The predicted amplitude was about 10°, and the frequency about 15 cycles/second in the region of maximum heating and deceleration.

vective and radiative heat transfer increase with air density and vehicle velocity, and are thus most severe when high velocities are allowed to persist into the lower atmosphere.

Below about 300,000 ft altitude, the atmosphere is dense enough to give an effective continuum type of flow. Here a shock wave occurs ahead of the body and the thermal energy appears in the hot 'shocked' air between the shock wave and the body. Passage through the shock wave increases the air density by a factor of ten or so, increases the temperature ten- to fifty-fold, and causes appreciable dissociation and some ionization. Heat is transferred from this heated region to the vehicle surface by convection (and conduction) through the viscous boundary layer and by radiation from the hot gas. When the boundary layer is of the laminar type (say above about 100,000 ft altitude), the convective heating rate per unit frontal area may be approximated, for relatively blunt bodies, as[4]

$$\left(\frac{q}{A_c}\right)_{LC} = \frac{3}{\sqrt{\left(\frac{Re}{Md}\right)_{SL} d}} \frac{\rho_{SL}}{2} \sigma^3 \qquad (3)$$

It will be noted that this indicates a variation in heating rate per unit surface area with the sine of the angle of surface inclination. A turbulent boundary-layer condition, occurring in the lower atmosphere, results in heating rates which are higher by about an order of magnitude.

Surface heating by radiation from the hot-gas region is still somewhat a matter of conjecture. Preliminary work, however, indicates that it becomes appreciable only when very high velocities are allowed to persist into the lower atmosphere. For the present case it is judged negligible.

The heating rate increases during the initial stages of entry because of the increasing atmospheric density. However, it reaches a maximum value when the velocity has been reduced to about 80 per cent of its initial value where the rate of decrease of velocity overcomes the rate of increase of atmospheric density. Thereafter, the heating decreases as additional deceleration occurs. As described more extensively elsewhere [5] the aerodynamic heat input can be balanced by thermal radiation from a thin metallic skin providing the heating rate is low enough so that the maximum equilibrium surface temperature is allowable for the surface material. However, this requires a rather light body or a drag-brake device so as to provide deceleration high in the atmosphere. In the present case, for the sake of simplicity, such complexity is not desired. Therefore, the radiation technique of heat rejection has been discarded in favor of some means of heat absorption.

One possibility is the use of a thick metallic skin to absorb the heat by temperature rise. Such a system is not very efficient from a weight standpoint, however, absorbing only about 100 Btu/lb. [5] More efficient is the use of a surface material which absorbs heat by a phase change. Heat absorptions of the order of 1,000 to 5,000 Btu/lb or more appear to be obtainable through the use of a material which vaporizes. [5][7] For example, it has been estimated that the depolymerization of Teflon will absorb somewhat more than 1,000 Btu/lb, [6] other plastic materials yield values up to 5,000 Btu/lb, [7] and graphite gives a value in the order of 10,000 Btu/lb. Advanced ICBM re-entry body designs involve the use of such ablation systems, and the Jupiter currently uses such a system. The required weight of such a vaporizing surface material depends on the total heat input during atmos-

pheric penetration. If we integrate, for example, the laminar convective heating rate (Eq. (3)) over the time of entry, the total heat load is found to be:

$$\left(\frac{Q}{A}\right)_{LC} = \frac{3\sqrt{\pi}\,\rho_{SL} u_i^2 \operatorname{erf}\left(\sqrt{\frac{C_D A_c}{W \sin\gamma}\frac{\rho_{SL}}{\alpha}}\right)}{2\alpha \sin\gamma \sqrt{\frac{C_D A_c}{W \sin\gamma}\frac{\rho_{SL}}{\alpha}} \sqrt{\left(\frac{Re}{Md}\right)_{SL} d}} \tag{4}$$

and for a surface material having s heat absorption per unit weight, γ, the weight of cooling system is found to be, in ratio to the total weight,*

$$\frac{W_c}{W} = \frac{3\sqrt{\pi}\,u_i^2 \sqrt{\frac{C_D A_c}{W \sin\gamma}\frac{\rho_{SL}}{\alpha}} \operatorname{erf}\left(\sqrt{\frac{C_D A_c}{W \sin\gamma}\frac{\rho_{SL}}{\alpha}}\right)}{2C_D \lambda \sqrt{\left(\frac{Re}{Md}\right)_{SL} d}} \tag{5}$$

This equation yields the rather surprising conclusion that the cooling-system weight requirement increases with the drag-mass parameter. A somewhat similar expression can be derived for turbulent convective heating. A qualitative picture of the weight requirements for a cooling system or drag brakes is indicated in Fig. H-5 as a function of the drag-mass parameter. Two minima appear: one where the drag-mass parameter is slightly greater than that which would bring about heating in the lower atmosphere with consequent higher turbulent heating rates, the other where the drag-mass parameter is just large enough so that radiative heat transfer is possible and yet not large enough to require a large weight in drag brakes. To avoid the complexity of drag brakes, the first of these

*This, of course, presupposes that the ratio W_c/W is relatively small compared to unity, since the velocity variation, Eq. (1), assumes a constant mass. For larger values of the weight ratio, a meteor-type analysis which takes into account the changing mass would have to be used.

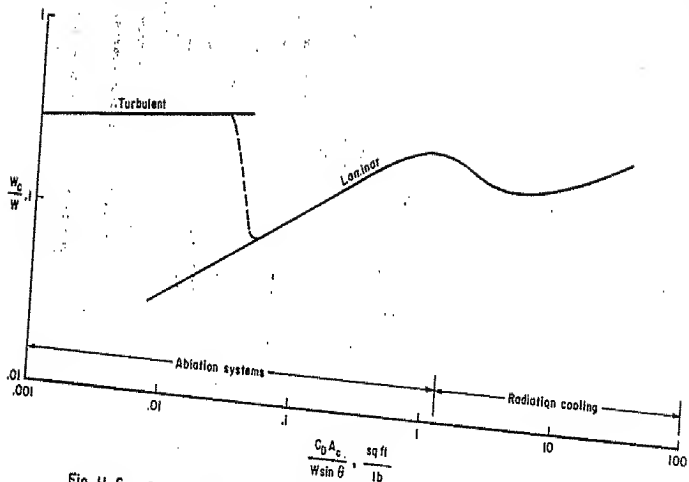

Fig. H-5 — Cooling system weight requirements for recoverable satellite vehicle

minima was chosen. The choice, as described previously, is an ellipsoidal body about 3 ft in diameter and weighing 250 lb at the beginning of re-entry.

Because of the shallow angle of atmospheric entry, the aerodynamic heating rates for this recovery are lower than those experienced by an ICBM re-entry body. However, the more gradual deceleration involves a longer time of heating so that the total heat load is greater, as Eq. (5) indicates. This means that a greater fraction of the total weight is required for heat protection. Thus, while only about 5 per cent of the total weight of an ICBM re-entry body may be ablated, the present case involves somewhat more than 10 per cent.

Using a vaporizing material with a heat-absorbing ability of 2,500 Btu/lb, about 35 lb of surface material is predicted to vaporize during descent. Using a relatively generous factor of safety, 65 lb of heat-absorbing surface has been postulated for this vehicle. This corresponds to an average thickness of about 3/8 in., with about one-half ablating and one-half remaining.

WATER IMPACT PHENOMENA[8]

In an initial program for the recovery of the satellite, it would be desirable to keep the return package as simple as possible. This would increase our ability to predict reliably the behavior of the vehicle during its re-entry. Therefore, a minimum of reliance should be placed on such devices as drag brakes, parachutes, reverse rockets and the like, just before impact. The satellite must survive impact on return to earth and the radio beacon must continue to operate after impact.

Analysis shows that the internal equipment can be protected and the deceleration loads kept to below 1,000 g's.

The payload, beacon and batteries are connected to the forebody by means of a properly chosen plastic, with properties compatible with the deceleration loads that can be tolerated by the internal components (several plastic materials with suitable combination of properties are available).

SYMBOLS FOR APPENDIX H

A_c	frontal (cross-sectional) area of body
A_s	surface area
C_D	drag coefficient
d	characteristic dimension of body
e	base of natural logarithms
g	gravitational acceleration
h	altitude
M	Mach number
q	heating rate
Re	Reynolds number, $du\rho/\mu$
u	velocity
u_i	velocity at initial entry condition
W	mass of body
x	distance
α	exponential coefficient in density relation, $\sigma = e^{-\alpha h}$
ρ	atmospheric density
ρ_{SL}	atmospheric density at sea level
σ	density ratio, ρ/ρ_{SL}
γ	path angle with local horizontal
μ	viscosity

Subscripts

LC	laminar connection

REFERENCES TO APPENDIX H

1. Huntzicker, J. H., H. A. Lieske, Physical Recovery of Satellite Payloads - A Preliminary Investigation (U), The RAND Corporation, Research Memorandum RM-1811, June 26, 1956 (Secret).

2. Gazley, Jr., C., D. J. Masson, A Recoverable Scientific Satellite, The RAND Corporation, Paper P-958 February 27, 1957.

3. Gazley, Jr., C., Deceleration and Heating of Bodies Entering a Planetary Atmosphere from Space, The RAND Corporation, Paper P-955, February 18, 1957.

4. Gazley, Jr., C., D. J. Masson, Recovery of a Circum-Lunar Instrument Carrier, The RAND Corporation, Paper P-1119, August 19, 1957.

5. Masson, D. J., C. Gazley, Jr., 'Surface-Protection and Cooling Systems for High-Speed Flight,' Aeron. Engr. Review, Vol. 15, No. 11, November 1956, pp. 46-55.

6. Porter, R. W., Recovery of Data in Physical Form, Franklin Institute Monograph No. 2, June 1956, pp. 103-112.

7. Masson, D. J., Mass-Transfer Cooling for Hypersonic Flight (U), The RAND Corporation, Classified Paper S-51, June 24, 1957 (Secret).

8. Masson, D. J., The RAND Corporation, Personal Communication, October 1957.